Visualizing the Dispersion of Internal Wave Beams in Density-Varying Fluid

Vohn Jacquez,[1, a)] Zachary Phan,[2] Zachary Taebel,[3] Dylan Bruney,[4] Pierre-Yves Passaggia,[5] and Alberto Scotti[6]

[1)] *Department of Physics and Astronomy, University of North Carolina at Chapel Hill, Chapel Hill, North Carolina 28223, USA*
[2)] *Department of Chemical and Biomolecular Engineering, North Carolina State University, Raleigh, North Carolina 27695, USA*
[3)] *Scripps Institution of Oceanography, University of California at San Diego, San Diego, California 92037, USA*
[4)] *Wake Forest University, Wake Forest, North Carolina 27109, USA*
[5)] *Laboratoire PRISME, Universite d'Orléans, Orléans, UPRES 4229, France*
[6)] *School for Engineering of Matter, Transport and Energy, Arizona State University, Tempe, Arizona 86287, USA*

[a)] Corresponding author: vbjacq8@unc.edu

Abstract. Physics curricula typically focus on electromagnetic, quantum, and standard mechanical waves propagating through media like air or taut strings. We investigated internal gravity waves, a peculiar type of mechanical wave that propagates through oceans and has significant geophysical implications. These dispersive waves obey a partial differential equation that accounts for the fluid density profile and buoyant force, resulting in a unique dispersion relation that couples their frequency directly to their angle of propagation. We explored this intricacy with a laboratory experiment to generate and observe internal waves in a more accessible environment than the ocean depths. In this experiment, we created and verified a linear saltwater stratification and applied an oscillatory topographic forcing. Because internal waves are invisible to the naked eye, we used background-oriented Schlieren optical techniques to track the density gradient and visualize wave propagation. Finally, we extracted a power spectrum of the density gradient to obtain the system's wave vector modes, quantitatively demonstrating the unique dispersive properties of internal waves.

INTRODUCTION

At the beach, onlookers may observe surface waves several meters high. Once they break, their energy shapes the shoreline. However, there also exist energetic waves that propagate below the surface. In this underwater abyss, these peculiar *internal waves* may span hundreds of meters, and their breaking instead shapes the distribution of nutrients, heat, and dissolved gases through vertical mixing. Their behavior has significant regional effects, including mitigating coral bleaching [1], nourishing ecosystems, and regulating melting rates of Arctic glaciers [2].

Beyond their environmental implications, internal waves are also peculiar mathematically. For example, they require stratified fluids (where density varies with height) to propagate. Their dispersion relation couples their frequencies directly to both the direction of propagation and the gradient of density, and their energy propagation is perpendicular to the phase propagation. Although the linear governing equation may resemble the classical wave equation, the buoyancy-restoring force associated with stable stratification produces this distinctive anisotropic dispersion relation [3, 4]. Our experiment specifically looked at the largest internal waves in our ocean, which are called *internal tides*. These waves arise when periodic tidal current flows over underwater ridges, converting barotropic tidal wave motion into baroclinic internal wave motion [5]. To emulate these waves and observe their unique behavior, we conducted a laboratory experiment that used a stratified tank and oscillatory forcing for wave generation, and optical analysis methods. These quick, inexpensive methods provide an accessible alternative to the costly field measurements and long research cruises typically required to study this phenomenon.

INTERNAL WAVE EQUATION SOLUTION

The internal gravity wave solution for stratified fluids is derived from the Euler equations, which describe momentum and mass conservation in an inviscid fluid. We simplified the equations to a solvable form with the following assumptions: First, the equations can be linearized by assuming small wave amplitudes. Second, since our stratification is weak, we invoked the Boussinesq approximation to characterize the density $\rho(z)$ as a reference density ρ_0 alongside a background density profile $\bar{\rho}(z)$ with small perturbations ρ', such that $\rho(z) = \rho_0 + \bar{\rho}(z) + \rho'$. Lastly, we assumed motion is restricted to a 2D plane. With these approximations, the following equation was derived for the velocity vector $\mathbf{u}(x,z,t)$, where (x,z) denote spatial coordinates and t is time:

$$\frac{\partial^2}{\partial t^2}\nabla^2\mathbf{u}+N^2\frac{\partial^2}{\partial x^2}\mathbf{u}=0. \tag{1}$$

Here, N refers to the Brunt-Väisälä frequency: $N=\sqrt{-\frac{g}{\rho_0}\frac{d\bar{\rho}(z)}{dz}}$ [6]. This is the frequency at which a fluid parcel oscillates when vertically displaced from its equilibrium (neutral buoyancy) position and thus measures the strength of our stratification. To seek solutions to Eq. (1), we substitute in a simple traveling wave of the form $\mathbf{u}(x,z,t)=\hat{\mathbf{u}}e^{i(kx+mz-\omega t)}$+c.c. to Eq. (1). Here, k and m are the wavenumber components of the trial wave solution we verify, and ω is the frequency. This leads to

$$\omega^2(k^2+m^2)\mathbf{u}-N^2k^2\mathbf{u}=0. \tag{2}$$

From Eq. (2), traveling waves are solutions to Eq. (1) provided their wavenumbers and frequency satisfy the *dispersion relation*:

$$\omega=N\sqrt{\frac{k^2}{k^2+m^2}}=N\sin\theta, \tag{3}$$

where θ is the angle from the horizontal at which the superposition of internal waves (wave group) propagates. One key consequence of Eq. (3) is that the wave group propagates perpendicularly to the phase velocity of its constituent modes (see Appendix B). Another key feature of this dispersion relation is that the frequency depends only on the ratio *m*/*k* and the Brunt-Väisälä frequency, not the wave vector's magnitude. Thus, waves of a given frequency must propagate at a fixed angle to the horizontal, independent of their wavelength. Conversely, a single frequency admits infinitely many wavelength modes (infinite degeneracy) corresponding to different magnitudes of the wave vector at the same angle. Because k and m are also sign-free, the waves are horizontally and vertically symmetric about the forcing. When $\theta=90°$, the maximum allowable frequency is reached: $\omega = N$. Interestingly, although the dispersion relation was derived for the velocity, it applies to all wave variables including the density perturbation ρ' (when plugging the solution for $\mathbf{u}$ into the linearized Euler equations, the other variables also follow complex exponential solutions). The consequence is that we can characterize wave motion through ρ', a quantity that we optically determined in our experiment.

METHODS

We first used a two-bucket method with pure rock salt to create the necessary linear stratification [7]. This required three tanks: a freshwater holding tank, a saltwater tank, and a wave tank (203 cm long, 46 cm tall, 8 cm wide). Setting a 1:2 ratio for the saltwater tank's inflow to outflow resulted in a linearly stratified density profile, which corresponded to a constant Brunt-Väisälä frequency and a constant wave angle θ. We verified our stratification by lowering a conductivity probe [see Fig. 1(b)] down one edge of the tank with a stepper motor. We mapped the readings using a conductivity-to-density spline fit, calibrated beforehand with saline solutions of known densities. We measured a Brunt-Väisälä frequency of $N=1.394$ rad s^{-1}.

To emulate internal tides, we needed an oscillatory forcing. However, replicating the reference frame of internal tides involves flowing water past a topography (typically done with an intensive oscillating wall or paddle [8]). Instead, we moved a partially submerged ridge in a periodic loop with a stepper motor to simulate flow over a bottom topography in the fluid's frame of reference [9]. Our model ridge took the form $h(x)=h_0\mathrm{sech}^2\left(\frac{x}{h_0}\right)-h_0\mathrm{sech}^2\left(\frac{l_0}{h_0}\right)$, with h_0 being the maximum height and l_0 being the half-length. With an acrylic stencil, we used a hot wire to trace the shape out of nonporous styrofoam, yielding $l_0=17.2$ cm and $h_0=3.1$ cm. We oscillated the topography at a constant frequency of $\omega_0=1.047$ rad s^{-1} with a stroke amplitude of 1.34 cm. More details of the setup can be found in [10].

We visualized the dispersive behavior of internal waves with background oriented Schlieren (BOS) imaging. BOS relies on the differing refractive indices of fluids with varied densities, a relationship that also causes desert mirages. As with mirages, observers viewing the tank see a distorted image of the background. To utilize this phenomena, we projected a random dot pattern on a flat surface 280 cm behind the tank. We used an array of high-resolution cameras (3312×2488 pixels) positioned 146 cm in front of the tank to capture photos of the full dot pattern at 2 Hz. By comparing the distortion across pictures, we estimated the gradient in density [11]. For further details on our setup and analysis, supplemental material is available on our GitHub repository [12].

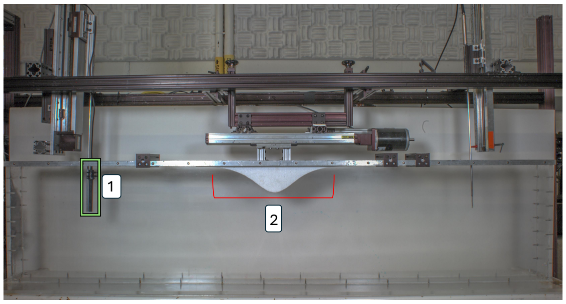

(a)

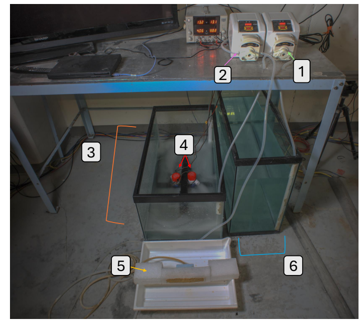

(b)

FIGURE 1. (a) Wave tank apparatus for internal wave generation and measurement. Casting a conductivity probe (1) yields a preexperiment Brunt-Väisälä frequency. Waves are formed by oscillating the topography (2) with a stepper motor. (b) Experimental setup utilizing the "two-bucket" method. Pumps 1 and 2 (1,2) move water through the saltwater and freshwater tanks (3,6) as bilge pumps (4) mix water in the saltwater tank. The diffuser (5) floats on the mixing tank surface as the mixture pumps in.

RESULTS AND DISCUSSION

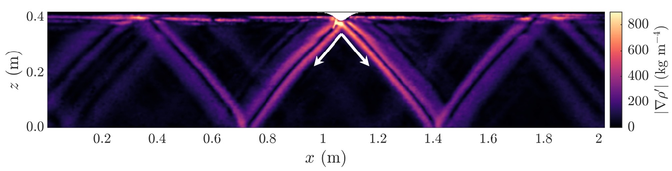

(a)

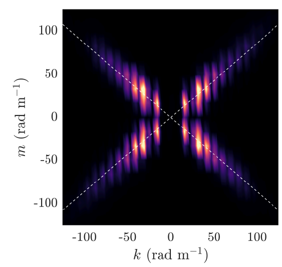

(b)

FIGURE 2. (a) Magnitude of the density perturbation gradient $|\nabla\rho'|$ (in $\mathrm{kg\cdot m^{-4}}$) obtained from BOS. The superimposed vector indicates the expected angle $\theta = 48.7°$ from the internal wave dispersion relation. Data were collected 7.5 min after the onset of forcing and smoothed using splines [13]. (b) The 2D power spectrum of $|\nabla\rho'|$ obtained using BOS as a function of wavenumbers (k,m). Dashed lines have a slope corresponding to the ratio of m/k set by Eq. (3) for linear internal waves at a single frequency. A Hann window of size 38.0 cm $\times$ 202.1 cm reduced spectral leakage. The final FFT resolution was 3.11 rad m^{-1} in x and 16.53 rad m^{-1} in z.

Our BOS visualization is shown in Fig. 2(a). Here, we observed that our forcing constructed not only a single sinusoidal wave, but rather a strong localized beam on the diagonals. To investigate this beam, we carried out a 2D FFT (fast Fourier transform) on the density perturbation fields and depicted the most prominent wave vectors in the system [Fig. 2(b)]. We found that there was not just one mode but multiple modes in each quadrant. Analogous to internal tide generation in the ocean (where forcing is at a tidal frequency but unspecified wavenumber), these modes corresponded to individual sinusoids generated by our forcing frequency, with the X pattern arising from sign freedom in both k and m and the constant ratio m/k set by ω_0 for all sinusoids. Thus, numerous sinusoidal modes with different wavelengths and amplitudes, yet with the same frequency, created a stable wavepacket with crests and troughs corresponding to the bright stripes present in 2(a). Because the modes shared the same frequency, the same angle must also be shared; the whole wave group propagated in the same direction with wave packets "stacked" down the diagonals. At the onset of forcing, the beam evolved by propagating throughout the tank, but the structure of the beam envelope remained in place. While wave packets in other areas of physics often disperse and lose their form (e.g., quantum free particles, photons in media), the wave group envelope is conserved with time. This stability is characteristic of linear internal wave regimes, confirmed through verification of the propagation angle predicted by Eq. (3), $\theta = 48.7°$ [shown by white arrows in Fig. 2(a)].

Although linear wave theory predicts that the wave packet's amplitude remains constant, we observed that the pattern was brightest nearest to the forcing, gradually dimming as it propagated away and reflected off the bottom.

This was due to shear instability and dissipation. Similarly, dimming can be observed in the corners of the X in the FFT, where higher modes (higher m and k) faded away.

Thus, by virtue of stratification and buoyancy, we observed how a single forcing mechanism created a wave beam: a wavepacket formed from the superposition of sinusoidal modes at one frequency. Unlike other waves in physics that unravel due to dispersion, we demonstrated how the internal wave beam propagated with a preserved shape and unified direction due to sharing a common frequency and angle via Eq. (3). The uniqueness of these waves is further emphasized when realistic physical conditions (i.e. boundary conditions and shear/viscosity) that real fluids are subjected to are considered.

CONCLUSION

Motivated by their peculiar mathematical and geophysical properties, we simulated internal tides in a laboratory setting with stratification and oscillatory forcing. Using BOS imaging, we demonstrated that the internal waves' dispersive behavior gave rise to a localized wave beam. There were numerous constituent modes at the same frequency that allowed for a stable, in-place superposition to form, as found in our 2D FFT results. This stable wave beam is characteristic of linear internal waves. We verified our operation in this regime by confirming our results agreed with the dispersion relation curves. In addition to stratification and buoyancy, we found that boundary conditions and non-conservative forces produced discretization and decoherence of the wave beam modes, emphasizing the uniqueness of an internal wave system.

More complex physical properties are exhibited in turbulent regimes, an object of further study. We predict that increasing the forcing's length scales or driving frequency could move the experimental system toward a *nonlinear* regime. One could also use BOS to extract where energies lie, as the emergence of nonlinearity disperses energy to new frequencies. These frequencies would form linearly independent wave vectors, leading to decoherence in the initial wave beam. With some effort, our setup could also be extended to include additional oceanographic dynamics such as double diffusion or rotation. The former could be achieved using sugar and salt as stratifying agents, while the latter requires mounting our setup on a rotating platform.

ACKNOWLEDGMENTS

This research is supported by NSF Award No. OCE-2405801, MOMS: A Minimal Ocean Mixing System. We thank Jim Mahaney and the UNC-CH JFL for experiment facilitation, as well as peers who helped review our paper.

REFERENCES

1. A. S. Wyatt, J. J. Leichter, L. T. Toth, T. Miyajima, R. B. Aronson, and T. Nagata, "Heat accumulation on coral reefs mitigated by internal waves," Nat. Geosci. **13**, 28–34 (2020).
2. P. Washam, K. W. Nicholls, A. Münchow, and L. Padman, "Tidal modulation of buoyant flow and basal melt beneath Petermann Gletscher ice shelf, Greenland," J. Geophys. Res. Oceans **125**, e2020JC016427 (2020).
3. A. Gill, *Atmosphere-Ocean Dynamics*, Atmosphere-Ocean Dynamics, Vol. 30 (Elsevier Science, 1982) p. 131.
4. J. Lighthill, *Waves in Fluids*, Vol. 13 (Cambridge University Press, Cambridge, England, 2002) p. 1501.
5. C. B. Whalen, C. De Lavergne, A. C. Naveira Garabato, J. M. Klymak, J. A. MacKinnon, and K. L. Sheen, "Internal wave-driven mixing: Governing processes and consequences for climate," Nat. Rev. Earth Environ. **1**, 606–621 (2020).
6. P. Kundu and I. Cohen, *Fluid Mechanics* (Academic Press, New York, 2010) p. 265.
7. G. Oster and M. Yamamoto, "Density gradient techniques,," Chem. Rev. **63**, 257–268 (1963).
8. L. Gostiaux and T. Dauxois, "Laboratory experiments on the generation of internal tidal beams over steep slopes," Phys. Fluids **19**, 028102 (2007).
9. P. Echeverri, M. Flynn, K. B. Winters, and T. Peacock, "Low-mode internal tide generation by topography: An experimental and numerical investigation," J. Fluid Mech. **636**, 91–108 (2009).
10. J. Vohn, Z. Phan, Z. Taebel, D. Bruney, P.-Y. Passaggia, and A. Scotti, "A versatile laboratory approach to reproduce and analyze internal ocean wave dynamics," arXiv:2603.13512.
11. P.-Y. Passaggia, V. K. Chalamalla, M. W. Hurley, A. Scotti, and E. Santilli, "Estimating pressure and internal-wave flux from laboratory experiments in focusing internal waves," Exp. Fluids **61**, 1–29 (2020).
12. V. Jacquez, Z. Phan, Z. Taebel, D. Bruney, P.-Y. Passaggia, and A. Scotti, "InternalWavesSetup: Laboratory setup and analysis for internal-wave experiments," `https://github.com/vbjacq8/InternalWavesSetup` (2026).
13. D. Garcia, "Robust smoothing of gridded data in one and higher dimensions with missing values," Comput. Stat. Data Anal. **54**, 1167 (2010).

APPENDIX A

Another way we demonstrated the constraints imposed by the dispersion relation was by examining how the energy in the system is distributed with respect to angles. This was possible by Fourier transforming in space and time to obtain a spectrum as a function of frequency and wavenumbers (there can be multiple wavenumbers for a given frequency in our system), and then averaging over thin wedges of θ. The resulting plot is shown in Fig. 3.

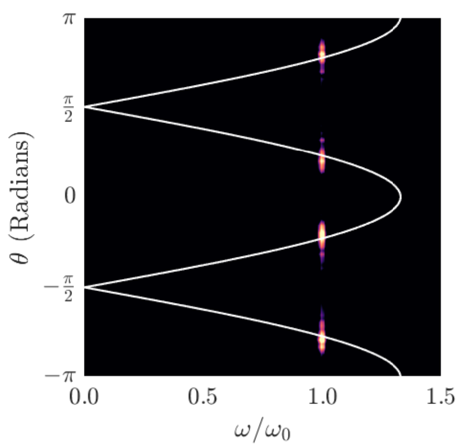

FIGURE 3. 2D power spectrum averaged over thin angles to convert k and m dependence to θ dependence, obtaining a spectrum with respect to angle of incidence and normalized frequencies. The solid white line corresponds to frequencies and propagation angles that agree with the dispersion relation.

Here, spectral amplitudes have peak values at (ω, θ) pairs consistent with the dispersion relation. The activity is located where the dispersion relation holds, and the four bright spots along the forcing frequency correspond to the four possible beam angles (one for each "quadrant," recalling that k and m are sign-free). These four peaks emphasized how reflections off the domain boundaries contributed to the wave beam's superposition.

APPENDIX B

The result from Eq. (3) may initially appear confusing because $\frac{k}{\sqrt{k^2+m^2}}$ should represent $\cos(\theta)$ instead of $\sin(\theta)$ if θ is the angle of the wave vector with respect to the horizontal. However, one characteristic of internal waves is that their group velocity propagates perpendicularly to their phase velocity. This can be shown by first defining the wave vector as

$$\mathbf{K} = (k,m). \tag{4}$$

Using these terms, the group velocity $\mathbf{v}_g$ is defined as

$$\mathbf{v}_g = \nabla_{\mathbf{K}}\omega = \left(\frac{\partial\omega}{\partial k}, \frac{\partial\omega}{\partial m}\right). \tag{5}$$

Using Eq. (3) to get an expression for $\omega(k,m)$, assuming $k > 0$ we take derivatives and arrive at the following:

$$\frac{\partial\omega}{\partial k} = \frac{Nm^2}{(k^2+m^2)^{3/2}} \tag{6}$$

and

$$\frac{\partial\omega}{\partial m} = -\frac{Nkm}{(k^2+m^2)^{3/2}}. \tag{7}$$

Now, the phase velocity is defined as

$$\mathbf{v} = \frac{\omega}{|\mathbf{K}|^2}\mathbf{K} = \frac{\omega}{k^2 + m^2}\mathbf{K}. \tag{8}$$

To check the orthogonality between $\mathbf{v}$ and $\mathbf{v}_g$, we take the inner product:

$$\mathbf{v} \cdot \mathbf{v}_g = 0. \tag{9}$$

This shows how the wave beam propagated perpendicularly to the wave phase, which can be seen in Fig. 2(a), where the wave beams traveled down the direction of the white arrows and the wave phase corresponded to the stripes in each beam. Since the group velocity is perpendicular to $\mathbf{K}$, there is a 90° offset: specifically, $\mathbf{K}$ uses $\cos(\theta)$ and $\mathbf{v}_g$ uses $\sin(\theta)$.